



# Correlation between the structural, magnetic, and dc resistivity properties of $\text{Co}_{0.5}\text{M}_{0.5-x}\text{Cu}_x\text{Fe}_2\text{O}_4$ ( $\text{M} = \text{Mg}$ , and $\text{Zn}$ ) nano ferrites

D. Parajuli<sup>1</sup> · Paulos Tadesse<sup>2</sup> · N. Murali<sup>3</sup> · K. Samatha<sup>4</sup>

Received: 28 August 2021 / Accepted: 13 December 2021 / Published online: 22 December 2021  
© The Author(s), under exclusive licence to Springer-Verlag GmbH, DE part of Springer Nature 2021

## Abstract

$\text{Cu}^{2+}$  substituted Co-Mg and Co-Zn mixed ferrite, nanoparticles with composition  $\text{Co}_{0.5}\text{M}_{0.5-x}\text{Cu}_x\text{Fe}_2\text{O}_4$  ( $x = 0.0, 0.2$  and  $0.4$ ) for  $\text{M} = \text{Mg}$  and  $\text{Zn}$  were produced by a sol–gel method involving auto-combustion. X-ray Diffraction (XRD), Fourier Transform Infrared (FTIR) Spectroscopy, Field effect scanning electron microscopy (FESEM) with EDS, Vibrating Sample Magnetometer (VSM), and Probe methods were used for determining the structural, electrical, and magnetic properties, DC electrical resistivity of these ferrites, respectively. The result of the lattice constant, crystallite size, particle size, bond lengths, magnetization, coercivity, and dc resistivity shows these spinel materials to be highly significant in everyday life.

**Keywords** Co-M-Cu mixed ferrite · XRD · FESEM · FTIR · VSM

## 1 Introduction

Ferrites nanoparticles and their composites are famous for their unusual but useful electric, magnetic, and adsorption properties used in recording devices, absorber, microwave device applications, cationic dyes, drug delivery, MRI applications, and sensors [1–8]. The ferrite nanoparticles with the general formula  $\text{AB}_2\text{O}_4$  have a spinel structure [9]. Cobalt ferrite  $\text{CoFe}_2\text{O}_4$  is partially inverted spinel structured hard ferrite. More  $\text{Co}^{2+}$  ions in the octahedral site [10] and  $\text{Fe}^{3+}$  ions are tetrahedral sites. The magnetic moment of  $\text{Fe}^{3+}$  ions and  $\text{Co}^{2+}$  ions are  $5\mu_B$  and  $3\mu_B$ , respectively [11]. The cation distribution in different sites plays an important role in the property of spinel. The interchange (A to B and half from B to A) of cations in the two interstitial sites gives rise to inverted spinel. The proportion of interchange determines

the resulting material properties [12, 13]. The partial substitution of Zinc in cobalt ferrite can produce sufficient positive changes in the properties of spinel structure like magnetic properties [14] and electrical resistivity for sensors and actuator applications [15]. Recent approaches like microemulsion, co-precipitation, ceramic, hydrothermal, sol–gel methods, etc., [16–19] help a lot in synthesizing the material of our interest. The easy and faster sol–gel method is used for ultrafine particles at room temperature [20]. Previously, we studied the effect of Cu substitution on the structural, magnetic, and dc electrical resistivity response of  $\text{Co}_{0.5}\text{Mg}_{0.5-x}\text{Cu}_x\text{Fe}_2\text{O}_4$  nano ferrites [21] and magnetic and dc electrical properties of Cu doped Co-Zn nano ferrites [22]. One-step solution combustion [23] and ultrasonic-assisted solvothermal [24] methods are also used for the synthesis of zinc and Cobalt ferrites. We have studied the Cu substituted NiZn ferrites [25, 26] and Nickel substituted CoZn ferrites [27] which show the significant improvement in their structural, morphological, magnetic and electric properties. In this work, we have comparatively analyzed both Co-Mg-Cu and Co-Zn-Cu mixed spinel nano ferrites.

The influence of M substitution on the magnetic and dc electrical resistivity properties of mixed ferrite  $\text{Co}_{0.5}\text{M}_{0.5-x}\text{Cu}_x\text{Fe}_2\text{O}_4$  ( $x = 0.0, 0.2$  and  $0.4$ ) ( $\text{M} = \text{Mg}$  and  $\text{Zn}$ ) is studied in this work.

✉ N. Murali  
muraliphda@gmail.com

<sup>1</sup> Research Center for Applied Science and Technology, Tribhuvan University, Kathmandu, Nepal

<sup>2</sup> Department of Physics, College of Natural Science, Arba Minch University, Arba Minch, Ethiopia

<sup>3</sup> Department of Physics, Andhra University College of Engineering (A), Andhra University, Visakhapatnam, Andhra Pradesh 530003, India

<sup>4</sup> Department of Physics, Andhra University, Visakhapatnam, Andhra Pradesh 530003, India

## 2 Experimental techniques

Cobalt nitrate hexahydrate ( $\text{Co}(\text{NO}_3)_2 \cdot 0.6\text{H}_2\text{O}$ ), Zinc nitrate hexahydrate ( $\text{Zn}(\text{NO}_3)_2 \cdot 6\text{H}_2\text{O}$ ), nickel nitrate ( $\text{Ni}(\text{NO}_3)_2 \cdot 6\text{H}_2\text{O}$ ), Magnesium nitrate hexahydrate ( $\text{Mg}(\text{NO}_3)_2 \cdot 6\text{H}_2\text{O}$ ), Iron nitrate nonahydrate ( $\text{Fe}(\text{NO}_3)_3 \cdot 9\text{H}_2\text{O}$ ), Cupric nitrate trihydrate ( $\text{Cu}(\text{NO}_3)_2 \cdot 0.3\text{H}_2\text{O}$ ), and Citric acid monohydrate ( $\text{C}_6\text{H}_8\text{O}_7 \cdot \text{H}_2\text{O}$ ) were used as starting materials without further purification. Double distilled water and ammonia ( $\text{NH}_3$ ) solution were also used as a solvent and to fix the pH value of the solution, respectively.

A stoichiometric amounts of nitrates were mixed with citric acid in a 1:1 M ratio to form Co-Mg-Cu and Co-Zn-Cu ferrites. When annealed at low temperature, the mixture gives rise to the single-phase ferrites, neutralized with ammonia ( $\text{pH} = 7$ ). The neutral solution was made clear solution with the help of deionized water and heated to  $150^\circ\text{C}$  until the formation of gel was converted into ash after the combustion and hence powdered. The powder was again sintered at  $1050^\circ\text{C}$  for 3 h, and pellets were prepared for characterization using Polyvinyl alcohol as a binder.

The structural analysis of all samples was conducted by using a Rigaku Miniflex II, USA- XRD diffractometer with  $\text{Cu K}\alpha$  radiation ( $\lambda = 1.5406 \text{ \AA}$ ) in the  $2\theta$  range of  $10^\circ$  to  $70^\circ$ . The morphology and compositional analysis of all samples were done by TESCAN- MIRA II LMH SEM, Czech Republic and Inca Oxford, Germany, respectively. The FT-IR measurements of all samples were also done using a Thermofisher, USA in the wavenumber range of  $350$  to  $1200 \text{ cm}^{-1}$ . Their magnetic properties at room temperature were also carried out by a EZ-VSM, Peru, and the DC resistivity of the samples was performed using four probe method (VTECH, India).

## 3 Results and discussions

### 3.1 XRD analysis

The XRD of Co-M-Cu ( $M = \text{Mg}$ , and  $\text{Zn}$ ) were taken separately using  $\text{CuK}\alpha$  radiation ( $\lambda = 1.5406 \text{ \AA}$ ) with the Bragg's angle ( $2\theta$ ) range  $10^\circ$ – $70^\circ$  with scan rate  $0.033^\circ\text{C}$  per second as shown in Fig. 1. The smooth and sharp peaks can confirm the crystalline nature of the sample in the XRD pattern, and the samples are pure spinel [28]. The respective planes' diffraction lines were compared with the standard JCPDS card No.08–0234 [29] for confirmation. Using the sharp peak (311) in Bragg's formula gives the value of interplanar spacing [30].

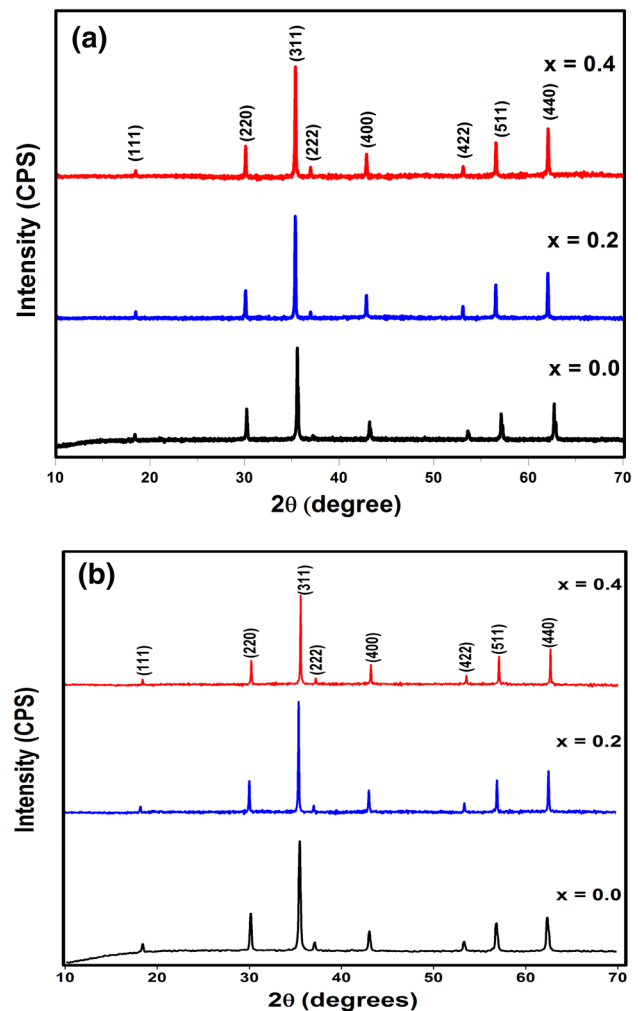


**Fig. 1** XRD design considered for **a** Co-Mg-Cu and **b** Co-Zn-Cu mixed spinel nano ferrites

The value of the lattice parameter is calculated using [31],

$$a = d_{hkl} \sqrt{h^2 + k^2 + l^2}$$
 where  $d_{hkl}$  is the interplanar spacing of hkl planes and is calculated by Bragg's law; here, the highest is obtained in (311).

The variation of 'a' with  $\text{Cu}^{2+}$  concentration in Co-M-Cu ( $M = \text{Mg}$  and  $\text{Zn}$ ) samples is shown in Fig. 2, and the values of lattice constant and crystallite size with their space group are listed in Table 1. The lattice constant for all the combinations decreases with concentration. The crystallite size for Co-Mg-Cu composition increase with concentration, while it first decreases and increases again for Co-Zn-Cu composition. In the plot, the lattice parameter is decreasing with increasing  $\text{Cu}^{2+}$  content. The elements with low spin ionic radii under consideration are Iron ( $0.61 \text{ \AA}$ ), Cobalt ( $0.65 \text{ \AA}$ ), Magnesium ( $0.72 \text{ \AA}$ ), Zinc ( $0.74 \text{ \AA}$ ), and Copper ( $0.73 \text{ \AA}$ ), respectively [32, 33]. So,

**Fig. 2** Variation of lattice constant and crystallite sizes with Co-Mg-Cu and Co-Zn-Cu mixed spinel nano ferrites

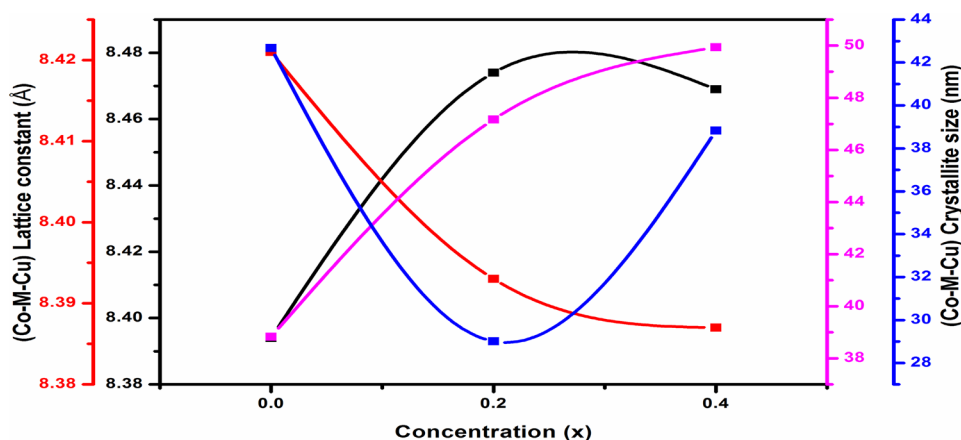


**Table 1** Lattice parameters and crystallite size of (a) Co-Mg-Cu and (b) Co-Zn-Cu mixed spinel nano ferrites

Parameters	Lattice constant (Å)			Crystallite size (nm)			Space Group	
	Concentration (x)	0.0	0.2	0.4	0.0	0.2		0.4
Co-Mg-Cu		8.394	8.474	8.469	38.83	47.17	49.94	<i>Fd-3 m</i>
Co-Zn-Cu		8.421	8.393	8.387	42.68	29.01	38.83	<i>Fd-3 m</i>

the lattice constant increases for Co-Mg-Cu systems and decreases for Co-Zn-Cu systems with concentration.

Debye-Scherrer’s formula gives the average size of the crystallite size [34].

$$D_{311} = \frac{0.9\lambda}{\beta \cos \theta}$$

where  $D_{311}$ ,  $\lambda$ ,  $\beta$ , and  $\theta$  are volume-averaged crystallite size, the wavelength of X-ray (1.5406 Å), full width at half maximum of (311) peak, and the diffraction angle, respectively.

The crystallite size depends on many factors like ionic radii, synthesis temperature, nucleation, etc. [35]. The increasing crystallite size in the Co-Mg-Cu composition indicates a substitutional solid solution of  $\text{Cu}^{2+}$ , and the size first decreases. Then rising in Co-Zn-Cu suggests substitutional first and transfer of toward the interstitial sites takes place or cations redistribution [36]. The crystallite size variation is seen in the XRD pattern.

The variation of lattice parameters and crystallite size indicates that  $\text{Cu}^{2+}$  is well introduced in the composition and does not alter the structure of this compound irrespective of its size. Even there are no impurities peaks in the XRD pattern indicating the single-phase compounds. Also, all the patterns are with space group *Fd-3 m* according to the JCPDS card number.

### 3.2 Field effect scanning electron microscopy studies

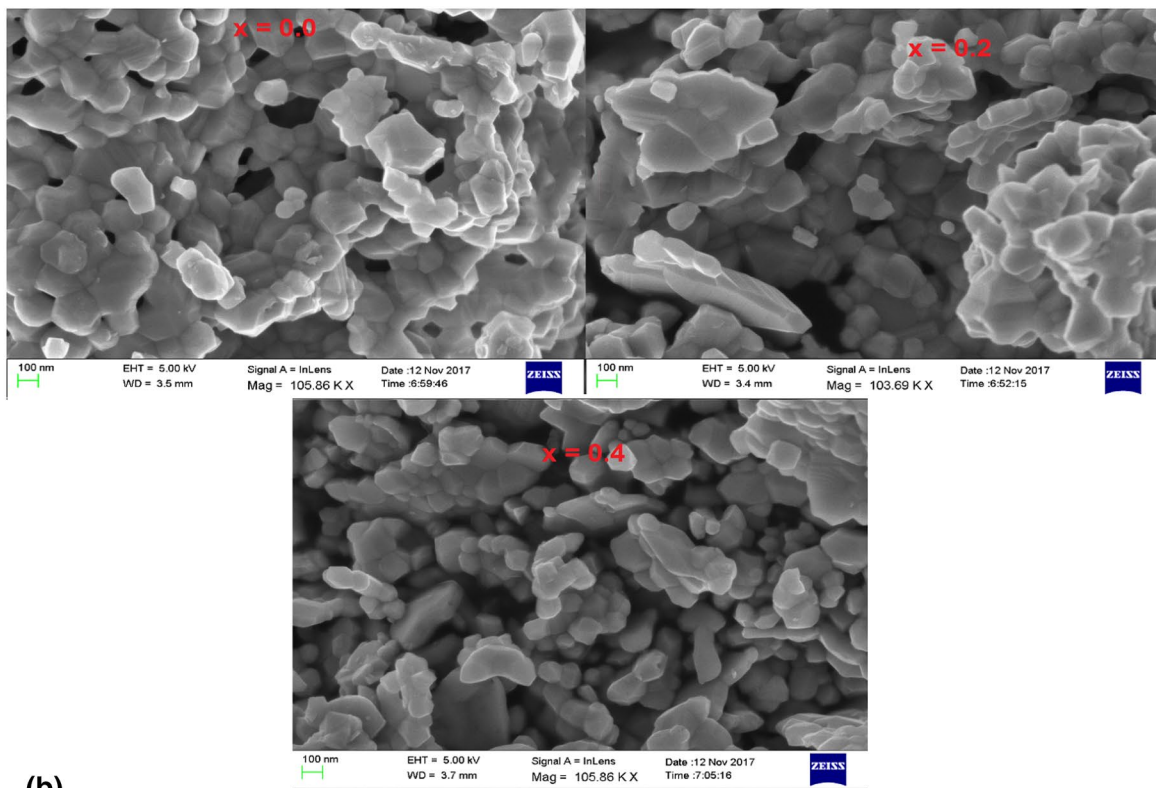
The images obtained from FESEM showing morphology and microstructure are shown in Fig. 3a and b. Initially,

the molecules seem more or less round with some agglomeration between them. The grain sizes first increase and decrease in Co-Mg-Cu composition, while it first decreases and increases in Co-Zn-Cu with the increase of  $\text{Cu}^{2+}$  cations. A sol-gel burning strategy obtains the fine-grained microstructure of all mixed ferrites [37]. A. Ghasemi et al. [38] and Z. Yue et al. [39] watched a similar impact with  $\text{Cu}^{2+}$  substitution. The porosity and agglomeration diminish with Cu content which is usual in ceramic materials [40]. The EDS spectra confirm the stoichiometric combination of the (a) Co-Mg-Cu and (b) Co-Zn-Cu mixed ferrites systems as shown from Fig. 4a and b.

### 3.3 FTIR studies

Normally, the spinel ferrites (a) Co-Mg-Cu and (b) Co-Zn-Cu mixed ferrites systems have a wavenumber range from 400 to 600  $\text{cm}^{-1}$ . Their mean distance of anion oxygen and metal cations in the tetrahedral and octahedral sites are found to be 1.89 Å and 1.99 Å in, respectively. This is the main reason for having two absorption bands for a ferrite at the two sites [41]. The decrease in site radius or bond length increases the fundamental frequency. As a result, the center of frequency shifted toward the high-frequency site [42]. This confirms the occupancy of  $\text{Cu}^{2+}$  in the octahedral site. There is also the possibility of migrating some  $\text{Cu}^{2+}$  from B to A in this particular concentration range. The values of the two absorption bands for the mentioned composition for different concentrations of  $\text{Cu}^{2+}$  are listed in Table 2, and their respective IR spectra are shown in Fig. 5a and b, respectively.

(a)



(b)

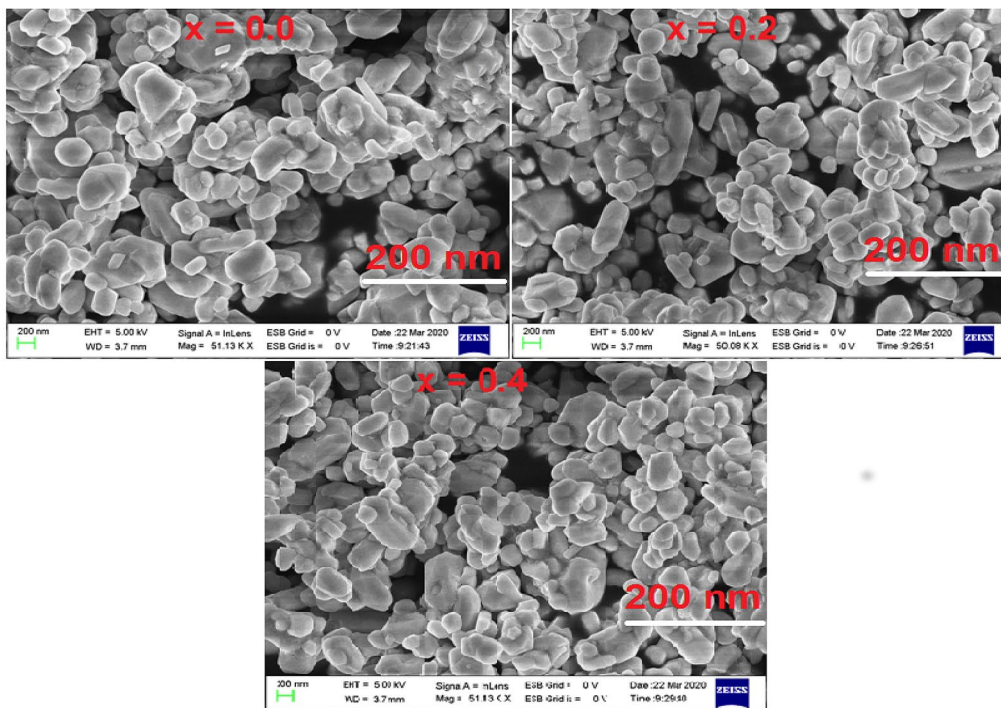
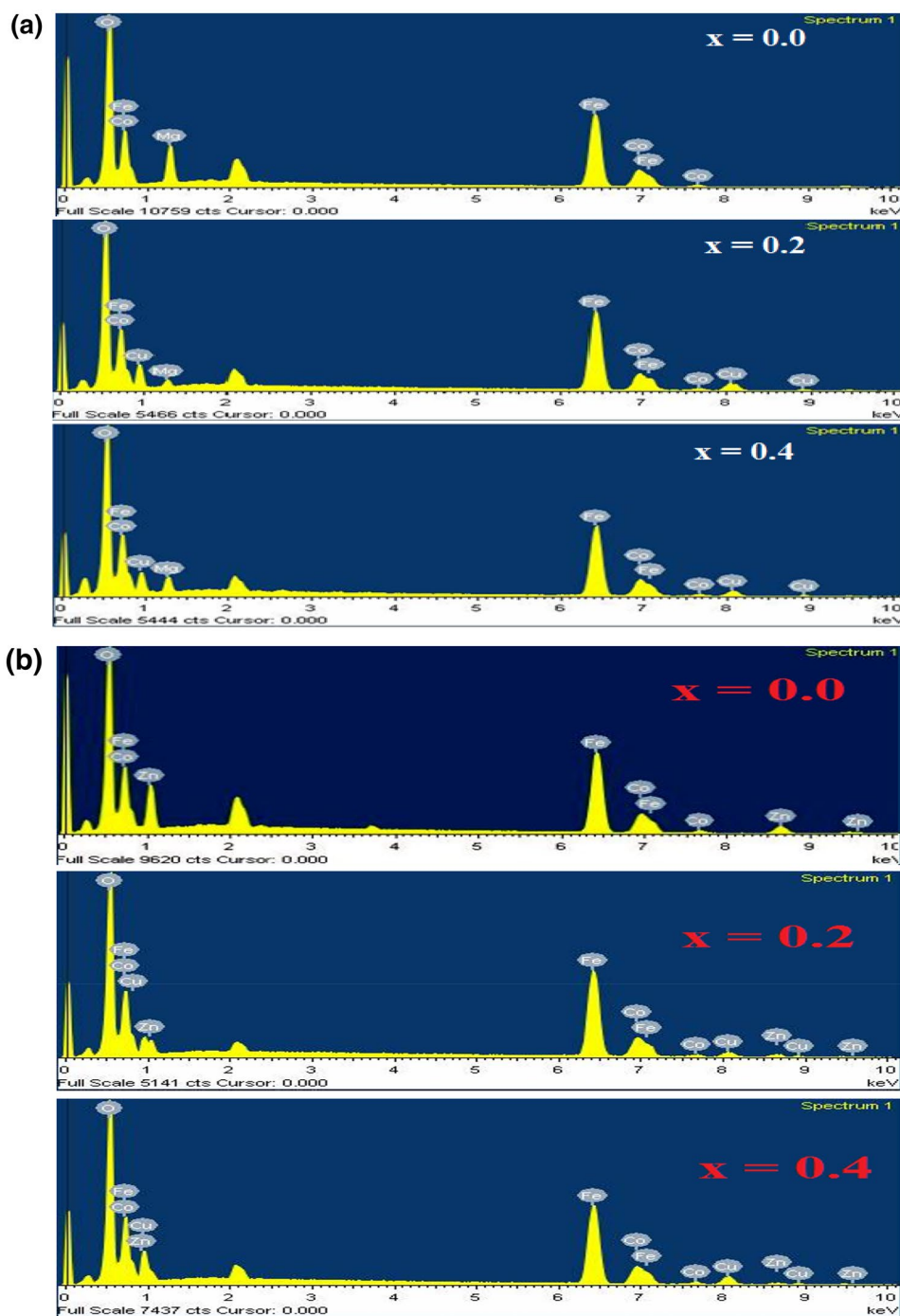


Fig. 3 FESEM images of **a** Co-Mg-Cu and **b** Co-Zn-Cu mixed spinel nano ferrites



**Fig. 4** EDS spectra of **a** Co-Mg-Cu and **b** Co-Zn-Cu mixed spinel nano ferrites



**Table 2** Tetrahedral ( $\nu_1$ ) and Octahedral ( $\nu_2$ ) absorption bands of Co-Mg-Cu, and Co-Zn-Cu mixed ferrites

Concentration (x)	0.0		0.2		0.4	
	$\nu_1$ (cm <sup>-1</sup> )	$\nu_2$ (cm <sup>-1</sup> )	$\nu_1$ (cm <sup>-1</sup> )	$\nu_2$ (cm <sup>-1</sup> )	$\nu_1$ (cm <sup>-1</sup> )	$\nu_2$ (cm <sup>-1</sup> )
Co-Mg-Cu	587.32	401.91	580.23	357.09	585.58	389.84
Co-Zn-Cu	524.661	399.28	579.633	378.99	579.634	393.49

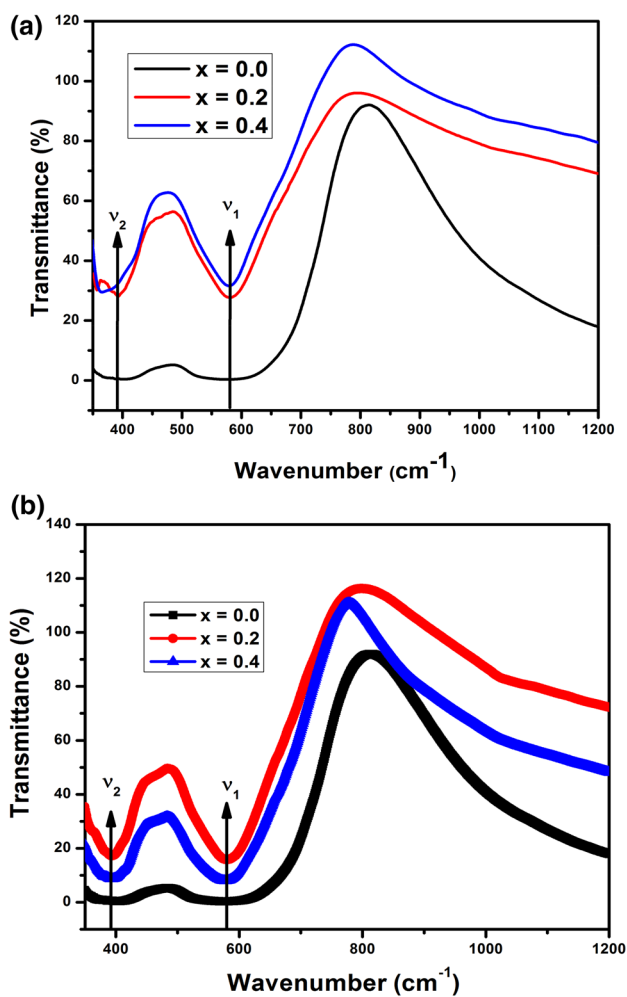


**Fig. 5** Infrared spectra of **a** Co-Mg-Cu and **b** Co-Zn-Cu mixed spinel nano ferrites

The general trend of transmittance is increasing with the concentration. All the compositions are mixed ferrites. The octahedral frequency is below  $400\text{ cm}^{-1}$ , which may be due to the decrease in site radius and vibration with the increment in non-magnetic  $\text{Cu}^{2+}$  concentration. The decrease in site radius decreases the unit cell dimension and decreases the wavenumber or increases the fundamental frequency [43]. This is how the absorption band on the octahedral site has shifted toward the lower wavenumber side, i.e., below  $400\text{ cm}^{-1}$ .

### 3.4 Magnetic properties

The Saturation magnetization ( $M_s$ ), Remnant magnetization ( $M_r$ ), and Coercive field ( $H_c$ ) of Co-Mg-Cu and Co-Zn-Cu mixed ferrites are listed in Table 3. Figure 6a and b show the room temperature hysteresis loops of Co-Mg-Cu and Co-Zn-Cu mixed ferrites, respectively. Here, the coercivity first decreases and then increases for Co-Mg-Cu and first increases and then decreases for Co-Zn-Cu, respectively, with the Copper concentration as shown in Fig. 7. According to the AB-BA exchange interaction effect, the substitution of  $\text{Fe}^{3+}$  by  $\text{Cu}^{2+}$  ions at the tetrahedral site increased the total magnetization of the sample [44]. The magnetic ordering in B sublattice is of uniform triangular type. In a semi-disordered system like Co-Zn ferrite, sudden tilting, or overturning effect (canting) in magnetic moments decreases the magnetization.  $M_A$  and  $M_B$  represent the magnetic saturation at tetrahedral and octahedral sites [45]. The difference in the magnetic moments in the two sites gives a net magnetic moment [46]

$$M_s = |M_A - M_B|$$

Moreover, the coercivity decreases with the concentration of  $\text{Cu}^{2+}$ .  $M_s$  depends on size if the number of atoms on the surface is remarkable to the total number of the sample volume. The lower value of  $M_s$  indicates the surface effect that makes the magnetic moments non-collinear, ferrimagnetically aligned spin [47].

### 3.5 DC electrical resistivity

The dc resistivity ( $\log \rho$ ) versus temperature ( $10^3/T$ ) plot of M (=Mg, and Zn) substituted  $\text{Co}_{0.5}\text{M}_{0.5-x}\text{Cu}_x\text{Fe}_2\text{O}_4$  ( $x=0.0, 0.2$  and  $0.4$ ) ferrites are shown in Fig. 8a and b, respectively. The inverse proportionality of the resistivity with temperature, i.e., the negative temperature coefficient with resistance or the semiconducting property, is seen [48]. Here, the drift mobility of the charge carriers is increased by heating which creates the hopping of electrons from  $\text{Fe}^{3+}$  to  $\text{Fe}^{2+}$  ions. Such ions pairs depend on the sintering condition and the number of  $\text{Fe}^{3+}$  to  $\text{Fe}^{2+}$  ions. The DC electrical resistivity monotonically decreases for Co-Mg, and first increases then decrease for Co-Zn with  $\text{Cu}^{2+}$  concentration in all the compositions.

**Table 3**  $M_s$ ,  $M_r$ , and  $H_c$  of Co-Mg-Cu, and Co-Zn-Cu mixed ferrites

Concentration (x)	0.0			0.2			0.4		
	$M_s$ (emu/g)	$M_r$ (emu/g)	$H_c$ (Oe)	$M_s$ (emu/g)	$M_r$ (emu/g)	$H_c$ (Oe)	$M_s$ (emu/g)	$M_r$ (emu/g)	$H_c$ (Oe)
Co-Mg-Cu	13.81	4.24	321.06	42.95	12.4	264.14	23.64	11.9	959.65
Co-Zn-Cu	90.13	11.23	176.24	41	11.8	408.3	57	6.3	120.2

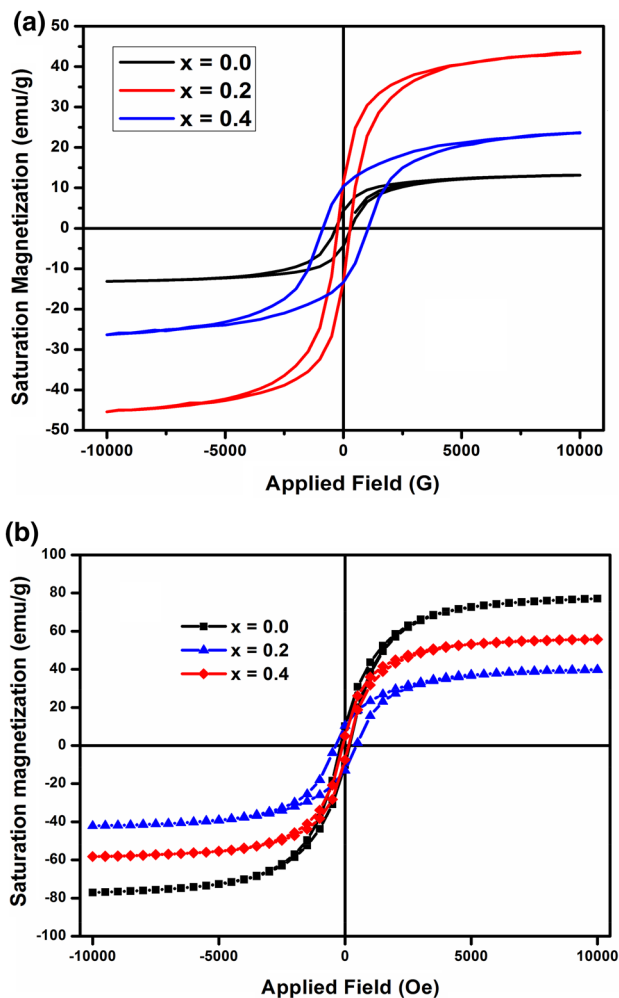
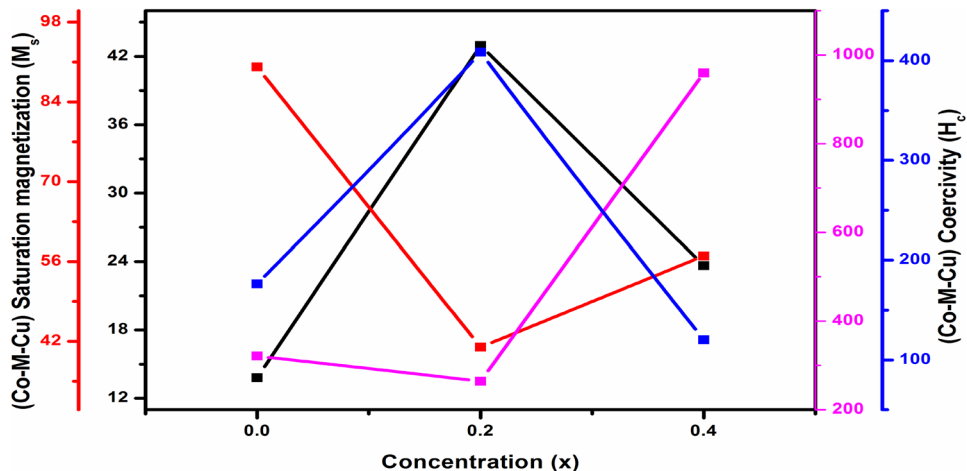


Fig. 6 Hysteresis loops of a Co-Mg-Cu and b Co-Zn-Cu mixed spinel nano ferrites at room temperature

Fig. 7 The saturation magnetization ( $M_s$ ) and Coercivity ( $H_c$ ) plot of Co-Mg-Cu and Co-Zn-Cu mixed spinel nano ferrites at room temperature



The resistivity of samples is calculated from the slopes of the plots of the ferrite samples. The resistivity of the samples is higher in their bulk and higher density or lower porosity [49]. The relationship between resistivity and temperature may be expressed as [50]

$$\rho = \rho_o e^{-\left(\frac{\Delta E}{KT}\right)}$$

$\rho_o$  and  $\rho$  are the resistivity at 0 and T K, respectively.  $\Delta E$ , K, and T are the activation energy, Boltzmann constant, and absolute temperature.

The mode of activation energy decreases for Co-Mg-Cu and first increases, then decreases for Co-Zn-Cu mixed ferrites with  $Cu^{2+}$  concentration, as shown in Fig. 9. In the figures, the resistivity or activation energy increases up to  $x=0.2$  attention and decreases in Co-Zn-Cu indicate that the ferrite has a semiconducting gap [51].

### 4 Conclusion

XRD, SEM-EDS, FTIR show their spinel structures and agrees with the previous results. XRD shows that the lattice constant for all the combinations decreases with concentration. The crystallite size for Co-Mg-Cu composition increase with attention, while it first decreases and increases again for Co-Zn-Cu composition. In the plot, the lattice parameter is decreasing with increasing  $Cu^{2+}$  content. FESEM shows that the un-doped molecules seem more or less round with some agglomeration between them. The grain sizes first increase and reduce Co-Mg-Cu composition, while it first decreases and increases in Co-Zn-Cu with the increase of  $Cu^{2+}$  cations. The porosity and agglomeration diminish with  $Cu^{2+}$  content, which is usual in ceramic materials. FTIR shows that the general trend of transmittance is increasing with the concentration. All the compositions are mixed ferrites with a wavenumber range of 400–600  $cm^{-1}$ . The absorption

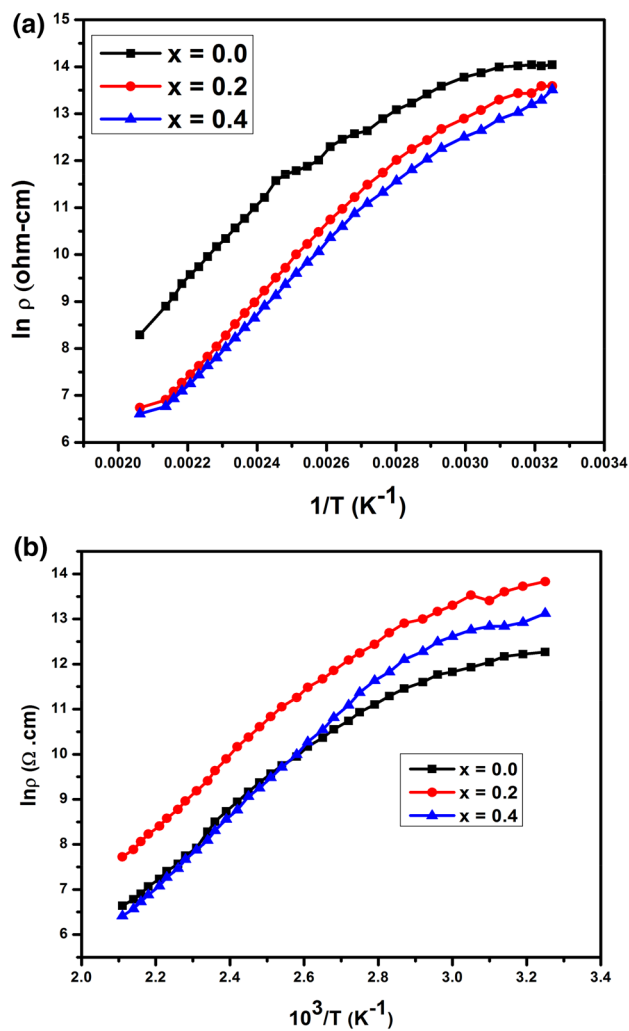


**Fig. 8** Temperature versus DC electrical resistivity of **a** Co-Mg-Cu and **b** Co-Zn-Cu mixed spinel nano ferrites

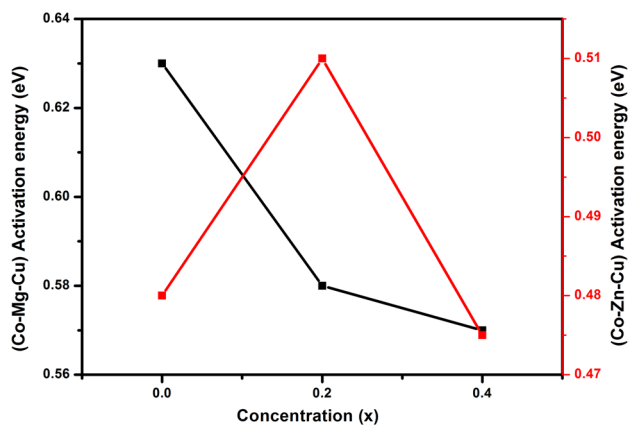


**Fig. 9** Activation energy versus Cu concentration ( $x$ ) of Co-Mg-Cu and Co-Zn-Cu mixed spinel nano ferrites

band on the octahedral site has shifted toward the lower wavenumber side, i.e., below  $400\text{ cm}^{-1}$ , due to decreased ionic radius and vibration increment in non-magnetic  $\text{Cu}^{2+}$  concentration.

VSM shows that the coercivity first decreases then increases for Co-Mg-Cu. First, increases then decrease for Co-Zn-Cu, respectively, with the concentration of Copper. According to the AB-BA exchange interaction effect, the substitution of  $\text{Fe}^{3+}$  by  $\text{Cu}^{2+}$  ions at the tetrahedral site increased the total magnetization of the sample. The canting impact is seen on the semi-disordered system like Co-Zn ferrite, which decreases the magnetization.  $M_s$  depends on size if the number of atoms on the surface is remarkable for the total number of the sample volume. The lower value of  $M_s$  indicates the surface effect that makes the magnetic moments non-collinear on the surface, a ferrimagnetically aligned spin. Generally, the activation energy decreases with conducting Copper concentration, and all the composition shows the semiconducting behavior in de resistivity plot. In Co-Zn-Cu, the resistivity or activation energy first increases up to  $x = 0.2$  concentration and decreases, indicating the effective semiconducting gap in this ferrite.

**Acknowledgements** This research received no external funding.

## Declarations

**Conflict of interest** The author(s) declare that they have no conflict of interest.

## References

1. T. Roman, R.L. Asavei, N.E. Karkalos, C. Roman, C. Virlan, N. Cimpoesu, B. Istrate, M. Zaharia, A.P. Markopoulos, K. Kordatos, S. Stanciu, A. Pui, *Int. J. Appl. Ceram. Technol.* **16**, 693 (2019)
2. V. Raghavendra, G. Raju, M. Gnana Kiran, M.S.N.A. Prasad, E. Rajesh, G. Pavan Kumar, N. Murali, *Results Phys.* **12**, 947 (2019)
3. C. Virlan, R.G. Ciocârlan, T. Roman, D. Gherca, N. Cornei, A. Pui, *Acta Chem. Iasi.* **21**, 19 (2013)
4. T. Vidya Sagar, T. Subba Rao, K. Chandra Babu Naidu, *Mater. Chem. Phys.* **258**, 123902 (2021)
5. E. Myrovali, N. Maniotis, A. Makridis, A. Terzopoulou, V. Ntomprougkidis, K. Simeonidis, D. Sakellari, O. Kalogirou, T. Samaras, R. Salikhov, M. Spasova, M. Farle, U. Wiedwald, M. Angelakeris, *Sci. Rep.* **6**, 1 (2016)
6. D. Parajuli, V. Raghavendra, B. Suryanarayana, P. Anantha Rao, N. Murali, P.V.S.K. Phanidhar Varma, R. Giri Prasad, Y. Ramakrishna, K. Chandramouli, *Results in Phys.* **23**, 103947 (2021)
7. K. Ramanjaneyulu, B. Suryanarayana, V. Raghavendra, N. Murali, D. Parajuli, K. Chandramouli, *Solid State Technol.* **64**, 7192 (2021)
8. P.V.S.K. Phanidhar Varma, V. Raghavendra, D. Parajuli, N. Murali, K. Chandramouli, *Solid State Technol.* **63**, 8820 (2020)
9. S.K. Kumar, N. Murali, D. Parajuli, A. Ramakrishna, P.S.V. Subba Rao, M.P. Rao, *Solid State Technol.* **63**, 4069 (2020)
10. S.Y. Mulushoa, N. Murali, M.T. Wegayehu, V. Veeraiah, K. Samatha, *Mater. Today: Proc.* **13**, 26460 (2018)



11. K. Chandramouli, V. Raghavendra, P.V.S.K.P. Varma, B. Suryanarayana, T.W. Mammo, D. Parajuli, P. Taddesse, N. Murali, *Appl. Phys. A* **127**, 596 (2021)
12. A.I. Popov, Z.V. Gareeva, F.A. Mazhitova, R.A. Doroshenko, J. Magn. Magn Mater. **461**, 128 (2018)
13. N. Sangeneni, K.M. Taddei, N. Bhat, S.A. Shivashankar, J. Magn. Magn Mater. **465**, 590 (2018)
14. S. Lalwani, R.B. Marichi, M. Mishra, G. Gupta, G. Singh, R.K. Sharma, *Electrochim. Acta* **283**, 708 (2018)
15. L. Andjelkovic, M. Suljagic, M. Lakic, D. Jeremic, P. Vulic, A.S. Nikolic, *Ceram. Int.* **44**, 14163 (2018)
16. R.G. Ciocarlan, A. Pui, D. Gherca, C. Virlean, M. Dobromir, V. Nica, M.L. Craus, I.N. Gostin, O. Caltun, R. Hempelman, P. Cool, *Mater. Res. Bull.* **81**, 63 (2016)
17. G. Rekha, R. Tholkappian, K. Vishista, F. Hamed, *Appl. Surf. Sci.* **385**, 171 (2016)
18. P. Samoila, L. Sacarescu, A.I. Borhan, D. Timpu, M. Grigoras, N. Lupu, M. Zaltariov, V. Harabagiu, J. Magn. Magn Mater. **378**, 92 (2015)
19. H.M. Zhang, Z. Wang, J.J. Pei, Y. Gao, J. Sol. Gel Sci. Technol. **90**, 404 (2019)
20. C. Virlean, G. Bulai, O.F. Caltun, R. Hempelmann, A. Pui, *Ceram. Int.* **42**, 11958 (2016)
21. P. Himakar, K. Jayadev, D. Parajuli, N. Murali, P. Taddesse, S.Y. Mulushoa, T.W. Mammo, B.K. Babu, V. Veeraiah, K. Samatha, *Appl. Phys. A* **127**, 1 (2021)
22. P. Himakar, N. Murali, D. Parajuli, V. Veeraiah, K. Samatha, T.W. Mammo, K.M. Batoo, M. Hadi, E.H. Raslan, S.F. Adil, J. Electron. Mater. **50**, 3758 (2021)
23. A.R. Abbasian, M. Shafiee Afarani, One-step solution combustion synthesis and characterization of ZnFe<sub>2</sub>O<sub>4</sub> and ZnFe<sub>1.6</sub>O<sub>4</sub> nanoparticles. *Appl. Phys. A* **125**, 721 (2019)
24. Abbasian, Ahmad Reza, Zahra Lorfasaie, Masoud Shayesteh, and Mahdi Shafiee Afarani, Synthesis of cobalt ferrite colloidal nanoparticle clusters by ultrasonic-assisted solvothermal process, *J Aust Ceram Soc* **56**, (2020) 1119–1126
25. D. Parajuli, K. Samatha, J. Phys. Sci. BIBECHANA **18**(1), 128–133 (2020)
26. D. Parajuli, K. Samatha, J. Phys. Sci. BIBECHANA **18**(2), 80–86 (2021)
27. D. Parajuli, N. Murali, K. Samatha, *JNPS* **7**(2), 24–32 (2021)
28. S. Yonatan Mulushoa, M. Tulu Wegayehu, G. Tewodros Aregai, N. Murali, M. Sushma Reddi, B. Vikram Babu, T. Arunamani, K. Samatha, *Chem. Sci. Trans.* **6**, 653 (2017)
29. S. Yonatan Mulushoa, C. Vijaya Kumari, V. Raghavendra, K. Ephraim Babu, B.S.N. Murthy, K. Suribabu, Y. Ramakrishna, N. Murali, *Physica B Condens. Matter.* **572**, 139 (2019)
30. B. Madhavilatha, D. Parajuli, K. Jayadev, N. Ch Komali, V.V. Murali, K. Samatha, *Biointerface Res. Appl. Chem.* **2**, 1899 (2021)
31. K. Chandramouli, B. Suryanarayana, P.V.S.K. Phanidhar Varma, V. Raghavendra, K.A. Emmanuel, P. Taddesse, N. Murali, T. Wegayehu Mammo, D. Parajuli, *Results Phys.* **24**, 104117 (2021)
32. K. Chandramouli, P. Anantha Rao, B. Suryanarayana, V. Raghavendra, S. Jesus Mercy, D. Parajuli, P. Taddesse, S. Yonatan Mulushoa, T. Wegayehu Mammo, N. Murali, *J. Mater. Sci.: Mater. Electron.* **32**, 15754 (2021)
33. S. Jesus Mercy, N. Murali, A. Ramakrishna, Y. Ramakrishna, V. Veeraiah, K. Samatha, *Appl. Phys. A* **126**(11), 1–13 (2020)
34. P.K. Roy, J. Bera, J. Magn. Magn Mater. **298**, 38 (2006)
35. T. Wegayehu Mammo, N. Murali, Y. Mulushoa Sileshi, T. Arunamani, *Physica. B Condens. Matter.* **531**, 164 (2018)
36. N. Murali, S.J. Margarete, G. Pavan Kumar, B. Sailaja, S. Yonatan Mulushoa, P. Himakar, B. Kishore Babu, V. Veeraiah, *Physica B Condens. Matter.* **522**, 1 (2017)
37. A. Ramakrishna, N. Murali, T.W. Mammo, K. Samatha, V. Veeraiah, *Physica B Condens. Matter.* **534**, 134 (2018)
38. S.E. Shirsath, B.G. Toksha, R.H. Kadam, S.M. Patange, D.R. Mane, G.S. Jangam, A. Ghasemi, *J. Phys. Chem. Solids* **71**, 1669 (2010)
39. Qi. Xiwei, Ji. Zhou, Z. Yue, Z. Gui, L. Li, J. Magn. Magn. Mater. **251**, 316 (2002)
40. T.W. Mammo, C.V. Kumari, S.J. Margarete, A. Ramakrishna, R. Vemuri, Y.S. Rao, K.V. Prasad, Y. Ramakrishna, N. Murali, *Physica B Condens. Matter.* **581**, 411769 (2020)
41. A.G. Kolhatkar, A.C. Jamison, D. Litvinov, R.C. Willson, T. Randall Lee, *Int. J. Mol. Sci.* **14**, 15977 (2013)
42. G. Raju, N. Murali, M.S.N.A. Prasad, B. Suresh, D.A. Babu, M.G. Kiran, A. Ramakrishna, M.T. Wegayehu, B.K. Babu, *Mater. Sci. Technol.* **2**, 78 (2019)
43. A. Ramakrishna, N. Murali, S.J. Margarete, K. Samatha, V. Veeraiah, *Physica B Condens. Matter.* **530**, 251 (2018)
44. A.V. Knyazev, I. Zakharchuk, E. Lähderanta, K.V. Baidakov, S.S. Knyazeva, I.V. Ladenkov, *J. Magn. Magn Mater.* **435**, 9 (2017)
45. M.M. Mallapur, P.A. Shaikh, R.C. Kambale, H.V. Jamadar, P.U. Mahamuni, B.K. Chougule, *J. Alloys Compd.* **479**, 797 (2009)
46. A.V. Knyazev, I. Zakharchuk, E. Lähderanta, K.V. Baidakov, S.S. Knyazeva, I.V. Ladenkov, *J. Magn. Magn Mater.* **435**, 9 (2017)
47. K. Chen, L. Jia, X. Yu, H. Zhang, *J. Appl. Phys.* **115**, 17A520 (2014)
48. X. Ren, G. Xu, *J. Magn. Magn Mater.* **354**, 44 (2014)
49. A. Saini, A. Thakur, P. Thakur, *J. Mater. Sci.: Mater. in Electr.* **27**, 2816 (2016)
50. A. Stergiou, G. Litsardakis, *J. AIP Conf. Proc.* **1627**, 117 (2014)
51. M.D. Hossain, A.T.M.K. Jamil, M.R. Hasan, M.A. Ali, I.N. Esha, M. Sarowar Hossain, M.A. Hakim, M.N.I. Khan, *Mater. Res. Express* **8**, 046102 (2021)

**Publisher's Note** Springer Nature remains neutral with regard to jurisdictional claims in published maps and institutional affiliations.